CHEMISTRY OF MATERIALS

pubs.acs.org/cm

Article

Two-Dimensional Supramolecular Nanoarchitectures of Polypseudorotaxanes Based on Cucurbit[8]uril for Highly Efficient Electrochemical Nitrogen Reduction

Cai-Cai Zhang,[#] Xiaolu Liu,[#] Yu-Ping Liu,[*] and Yu Liu[*]

Cite This: *Chem. Mater.* 2020, 32, 8724−8732

Read Online

ACCESS | Metrics & More | Article Recommendations | Supporting Information

ABSTRACT: Supramolecular assemblies with two-dimensional (2D) topology have drawn great attraction in the development of functional materials through a modular approach. Herein, a novel organic 2D polypseudorotaxane has been constructed on the basis of cucurbit[8]uril (CB[8]) through host-stabilized charge-transfer (CT) interactions of naphthol-modified porphyrin (TPP-Np) and viologen derivatives (DMV). Interestingly, the 2D polypseudorotaxanes could serve as a platform for preparation of ultrafine Pt nanoparticles with favorable and homogeneous dispersion through a simple self-metallized process, leading to the formation of supramolecular hybrid materials (PtNPs@(CB[8]/DMV/TPP-Np)). Surprisingly, the PtNPs@(CB[8]/DMV/TPP-Np) could be applied to efficient electrochemical nitrogen reduction reaction, with a NH_3 yield rate up to 23.2 μg h^{-1} mg_{Pt}^{-1} at −0.2 V versus a reversible hydrogen electrode under ambient conditions. Notably, our results not only demonstrate the feasible construction of 2D polypseudorotaxanes but also deepen the understanding of structure−activity relationships in supramolecular nanoarchitectures, as well as pave an effective and low-energy input strategy for artificial nitrogen fixation.

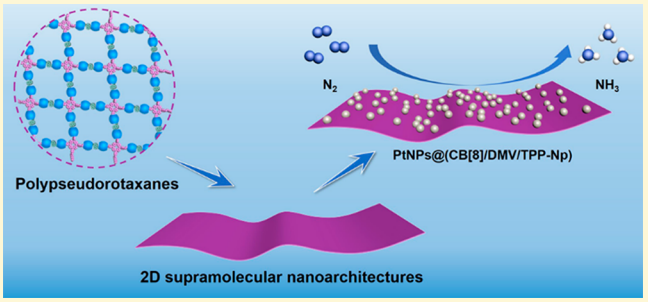

INTRODUCTION

Two-dimensional (2D) nanoarchitectures have drawn a great deal of attention in nanotechnology and materials science because of their fascinating physical and chemical properties as well as potential application in catalysis, electronics, sensing, separation, and other related fields.[1−3] To date, numerous efforts have been devoted to the formation and development of 2D nanoarchitectures. Among these various structures, organic 2D nanomaterials constructed through noncovalent interactions or supramolecular assembly were considered remarkable because of their flexible design routes, potential additional functionality, and highly modular nature.[4−7] Significantly, taking advantage of the host−guest interactions for the formation of stable (pseudo)rotaxanes or poly(pseudo)-rotaxanes, a series of 2D nanoarchitectures with a single-layer arrangement and high structural regularity were constructed. For instance, Li and Zhao reported remarkable results using mild conditions for the construction of 2D supramolecular organic frameworks (SOFs) in solution.[8] Moreover, Feng et al. utilized interface synthesis to obtain the large-area free-standing monolayers by host−guest enhanced donor−acceptor interactions.[9] In addition, our group designed photocontrolled and interconvertible 2D/1D supramolecular nanostructures with different fluorescence enhancement effects for Nile Red.[10] Recently, Scherman and Barrio reported platelet-like aggregates and 2D nanofibers undergo a stepwise self-assembly process.[11] Although the design and construct of 2D supramolecular nanoarchitectures of (pseudo)rotaxanes or poly-(pseudo)rotaxanes have been explored using diverse methods, their potential as reactors has rarely been studied, despite the fact that the 2D nanostructures have highly accessible active sites, homogeneous features, and large surface areas, which can provide a well-defined platform for substance formation and exchange.

On the other hand, integrating building blocks with special features into 2D nanoarchitectures to realize the generation of functional materials is becoming of widespread interest and general concern. In artificial systems, supramolecular assembly strategies using various noncovalent interactions provide the possibility to achieve optimal performance from simple elements under mild conditions, which is particularly important for the discussion of structure−activity relationships.[12] Porphyrin and its derivatives with unique physical, chemical, biological, and catalytic properties have attracted growing interest in the fields of nanotechnology and materials

Received: August 22, 2020
Revised: September 21, 2020
Published: October 2, 2020

https://dx.doi.org/10.1021/acs.chemmater.0c03425
Chem. Mater. 2020, 32, 8724−8732

science.[13−15] Because of significant and excellent features, a great deal of porphyrin-based nanostructures have been presented in the past decade.[16,17] In our previous work, we constructed a series of porphyrin-based supramolecular assemblies with well-defined morphologies, taking advantage of hydrophilic−hydrophobic as well as host−guest interactions.[18−20] Considering the topological characteristics of 2D nanomaterials, the design and synthesis of porphyrin-based 2D supramolecular nanoarchitectures are in high demand.

Herein, we report a convenient, facile, and modular approach for the construction of functional 2D polypseudorotaxanes in which a stable ternary complex could be formed on the basis of cucurbit[8]uril via host-stabilized charge-transfer (CT) interactions of naphthol-modified porphyrin and viologen derivatives. Because of the steric effect of macrocycles of cucurbit[8]uril, the 2D polypseudorotaxanes exit as single-layer films with a lateral size, in which porphyrin units prevent intermolecular aggregation. Interestingly, taking advantage of the photocatalytic properties of porphyrin, the 2D supramolecular nanoarchitectures can be self-metallized with Pt nanoparticles, enabling their further use as an excellent catalyst for electrochemical nitrogen reduction reaction with superior Faradaic efficiency and a satisfactory yield rate at −0.2 V vs RHE under ambient conditions, exhibiting high catalyst stability and excellent selectivity. The *in situ* Fourier transform infrared spectroscopic data indicated that the supramolecular system follows the associative mechanism during the nitrogen reduction reaction process. This work not only deepens the understanding of structure−activity relationships in 2D supramolecular nanoarchitectures but also opens up opportunities for the development of supramolecular polypseudorotaxanes to realize efficiency in electrochemical nitrogen reduction.

RESULTS AND DISCUSSION

Design and Synthesis of Naphthol-modified Porphyrin (TPP-Np) and Viologen Derivatives (DMV). Synthesis of the guest molecule TPP-Np was performed with commercially available 5,10,15,20-tetra(4-pyridyl)porphyrin. Salification was conducted in dimethylformamide at 90 °C for 12 h in a nitrogen environment with 2-(2-bromoethoxy)-naphthalene. Subsequently, the counterions were exchanged with chloride ions and ultimately give TPP-Np in yields of 60%.[21] Another guest molecule, DMV, was synthesized by the Zinke reaction, starting with 1,5-naphthalenediamine, which was reacted with 1-(2,4-dinitrophenyl)-4,4′-bipyridinium in ethanol and refluxed for 72 h. After methylation with methyl iodide and ion metathesis procedures, DMV was obtained as a yellowish solid. The detailed synthesis route of TPP-Np and DMV is shown in the Supporting Information. Characteristics for the design of TPP-Np and DMV as building modules, respectively, include the following: (i) Porphyrin as a functionalized group in the center of TPP-Np facilitates polypseudorotaxanes with photoactivity performance. (ii) The flexible hydrocarbon between the porphyrin core and naphthalene periphery in TPP-Np enables 2D supramolecular nanoarchitectures with pliable features. (iii) DMV as the linear connection element with a rigid structure provides the basic prerequisite for the formation of 2D supramolecular nanoarchitectures. Typically, cucurbit[8]uril, possessing a large cavity, is capable of simultaneously accommodating an electron-deficient guest and an electron-rich guest by host-stabilized CT interactions to form a 1:1:1 ternary complex with high association constants ($K_a \geq 10^{11}$ M^{-2});[22,23] the electron-rich unit naphthalene (Np) in TPP-Np and electron-deficient unit methylviologen (MV) in DMV could be simultaneously encapsulated in the cavity of CB[8] and provide the major driving force for the formation of 2D polypseudorotaxanes.

Construction and Characterization of 2D Polypseudorotaxanes. To ensure the formation of polypseudorotaxanes, we first explored the host−guest interactions between DMV and CB[8] by ^{1}H NMR experiments and UV/vis spectroscopy. As shown in Figure S12b, the signals for the protons of viologen units in DMV were significantly shifted upfield by addition of 2 equiv of CB[8]. This phenomenon provided evidence for the formation of a 2:1 inclusion complex between CB[8] and DMV, in which the viologen units were located in the cavity of the host and influenced by the shielding effect of CB[8]. The Job's plot was employed to find the binding stoichiometry of DMV and CB[8]. The top point of the curve appeared at the molar fraction X_{guest} = 0.33, indicating the 2:1 binding stoichiometry between CB[8] and DMV (Figure S13), which corresponds to the result of ^{1}H NMR experiments. Furthermore, the association constant (K_a) of DMV and CB[8] was calculated as $K_1 = 2.59 \times 10^4$ M^{-1}, $K_2 = 2.12 \times 10^4$ M^{-1} according to the result of UV/vis spectroscopic titrations (Figure S14). ^{1}H NMR experiments were utilized to collect information about the polypseudorotaxanes. With the addition of TPP-Np to a solution of CB[8]/DMV (Figure S12c), the signals of viologen units of DMV were further shifted upfield and broadened, meaning that a higher-level supramolecular assembly was formed. However, when the same operation was handled in D_2O solution of DMV alone, neither chemical shifts of the protons on DMV nor TPP-Np displayed, indicating that there was no obvious interaction between TPP-Np and DMV in the absence of CB[8] (Figure S15). According to the above experiment results, we believe that CB[8] can be employed as the module of the "molecular handcuff" to combine the two guest molecules together to form network-like polypseudorotaxanes.[24]

More detailed information on the polypseudorotaxanes was investigated by spectroscopy experiments. As shown in Figure 1, a remarkable intensity decrease was observed at peaks at 219 and 267 nm in the UV/vis spectra of CB[8]/DMV/TPP-Np compared to that of the individual components, which are attributed to the naphthalene units and viologen units, respectively. Moreover, there was an increase in the range of 450−700 nm, exhibiting the formation of the proposed polypseudorotaxanes via host-stabilized CT interactions. Fluorescence spectra provided further insight into the interactions between each part of the building blocks in the supramolecular nanoarchitectures. The peaks centered at 680 and 720 nm displayed a slight decline with the formation of polypseudorotaxanes, also suggesting cucurbit[8]uril is capable of drawing close the two guest molecules so that photoinduced electron transfer arises from the porphyrin moieties of TPP-Np to the viologen units of DMV (Figure S16).[25]

Dynamic light scattering (DLS), transmission electron microscopy (TEM), and atomic force microscopy (AFM) were subsequently utilized to identify the size and morphology of the 2D polypseudorotaxanes. The data from the DLS experiments indicate that the large size of CB[8]/DMV/TPP-Np formed indeed via CB[8]-mediated host−guest complexations, whereas there were no detectable signals in the solution of TPP-Np or CB[8]/DMV (Figures S17 and S18). TEM is an

https://dx.doi.org/10.1021/acs.chemmater.0c03425
Chem. Mater. 2020, 32, 8724−8732

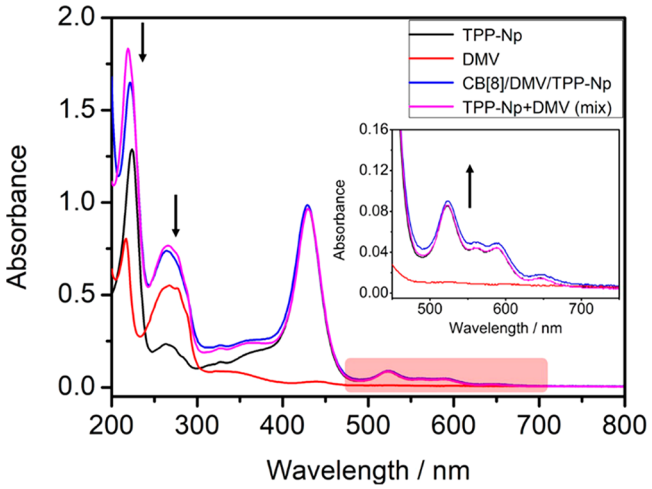

Figure 1. UV/vis spectra of TPP-Np ([TPP-Np] = 5×10^{-5} M, blank line), DMV ([DMV] = 1×10^{-4} M, red line), CB[8]/DMV/TPP-Np (CB[8]:DMV:TPP-Np = 2:1:0.5, [TPP-Np] = 5×10^{-5} M, blue line) and TPP-Np + DMV (TPP-Np:DMV = 0.5:1, [TPP-Np] = 5×10^{-5} M, purple line) in aqueous solution (light path = 1 mm).

efficacious method to intuitively characterize the morphology of the supramolecular assembly. As expected, the TEM images of CB[8]/DMV/TPP-Np indicate the formation of filmlike structures with some wrinkles, on account of the flexible structure between porphyrin and naphthalene units in TPP-Np (Figure 2A). The thickness of the nanomaterial is a very

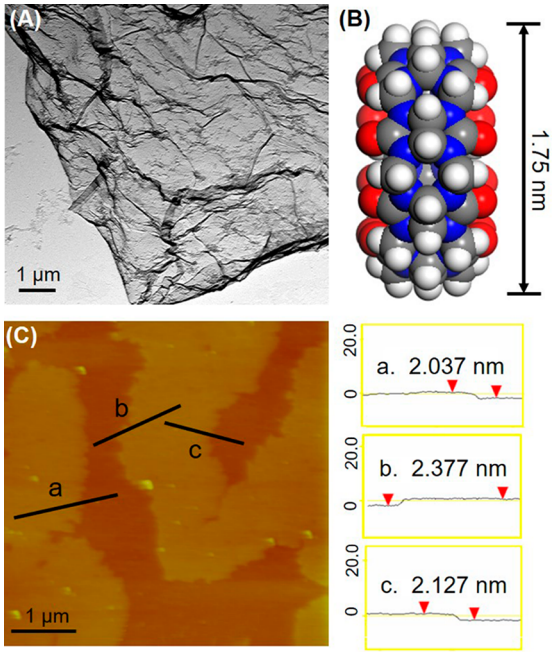

Figure 2. Characterization of 2D polypseudorotaxanes. (A) TEM image of CB[8]/DMV/TPP-Np. (B) Molecular size of CB[8]. (C) Tapping-mode AFM image of CB[8]/DMV/TPP-Np.

important parameter to evaluate the 2D nanostructures. Therefore, the as-prepared solution of CB[8]/DMV/TPP-Np was dropped onto a mica wafer and then investigated by tapping-mode AFM. As can be seen in Figure 2C, the graphene-like nanostructure of CB[8]/DMV/TPP-Np was observed by AFM. Cross-section analysis indicated that the height of the 2D supramolecular nanoarchitectures was symmetrical and uniform. The height of CB[8]/DMV/TPP-Np was measured to be ~2.2 nm at different positions, approaching the outer diameter of CB[8], strongly suggesting that the formation of single-layer 2D nanostructures resulted from a cross-link by CB[8].[26] Meanwhile, the CB[8] macrocycles effectively prevent the interlayer packing, leading to the 2D polypseudorotaxanes remaining as single-layer films with a lateral size. Moreover, for characterization of the fine microstructure arrangement inside the CB[8]/DMV/TPP-Np, grazing incidence small-angle X-ray diffraction (GI-SAXS) experiments were carried out. A sharp scattering peak corresponding to a *d* spacing of 4.1 nm is observed in Figure S19, which is assigned to the spacing of the quadrangular pores in the molecular model of the 2D polypseudorotaxanes, which is consistent with the proposed supramolecular assembly mode (Scheme 1).

Preparation and Characterization of PtNPs@(CB[8]/DMV/TPP-Np). Size-controlled and confined growth of such ultrafine metal nanoparticles have attracted extensive research interests because of excellent properties for applications in heterogeneous catalysis and electrocatalysis.[27,28] The porphyrin-based and well-defined 2D supramolecular nanoarchitectures have potential in the preparation of ultrafine Pt nanoparticles through a succession of light harvesting and photochemical cycles (Scheme S3).[29,30] First of all, platinum(II) solution was prepared by dissolving K_2PtCl_4 in ultrapure water under ambient conditions and was aged at least 24 h in the dark. The photoinduced reduction of platinum salts by CB[8]/DMV/TPP-Np was accomplished in the case of ascorbic acid as an electron donor under visible-light irradiation. Scanning electron microscope (SEM) images and TEM images show that the Pt nanoparticles were generated with uniform size (approximately 3 nm) and fine dispersion (Figure 3 and Figure S20). The high-resolution TEM image and selected area electron diffraction pattern exhibit the polycrystalline nature and characteristic diffraction rings of Pt nanoparticles. TEM-EDS also illustrated that Pt nanoparticles were prepared successfully (Figure S21). In addition, the Pt content in PtNPs@(CB[8]/DMV/TPP-Np) was estimated to be about 4.17 wt % based on ICP-AES measurement, which is consistent with the theoretical amount. As shown in FTIR spectra (Figure S22), the absorption at 3368 cm^{-1} assigned to the N−H stretching vibration in porphyrin units was obviously attenuated; meanwhile, the peak at 1722 cm^{-1} corresponding to C═O of cucurbit[8]uril stretching vibration shifted to 1715 cm^{-1}, suggesting that the Pt nanoparticles were immobilized by 2D polypseudorotaxanes. Furthermore, the Pt nanoparticles were characterized via X-ray photoelectron spectroscopy (XPS). The spectrum in the Pt 4f region showed peaks centered at 70.9 eV for Pt $4f_{7/2}$ and 74.2 eV for Pt $4f_{5/2}$, which could be assigned to Pt(0) (Figure S23).[31] However, no Pt nanoparticles were observed in the absence of the CB[8]/DMV/TPP-Np or without light irradiation. On the another hand, the obtained Pt nanoparticles were large in size and easy to reunite in the case of TPP-Np operating alone. The above control experiments demonstrated that the photoactivity of the porphyrin and the two-dimensional configuration of the CB[8]/DMV/TPP-Np are both critical for the development of functional supramolecular nanostructures.

Electrochemical Nitrogen Reduction Performance of PtNPs@(CB[8]/DMV/TPP-Np). Recently, the electrochemical nitrogen reduction reaction (NRR) to produce ammonia

https://dx.doi.org/10.1021/acs.chemmater.0c03425
Chem. Mater. 2020, 32, 8724−8732

Scheme 1. Schematic Illustration of the Construction of the 2D Polypseudorotaxanes Based on CB[8] via Host-Stabilized Charge-Transfer (CT)

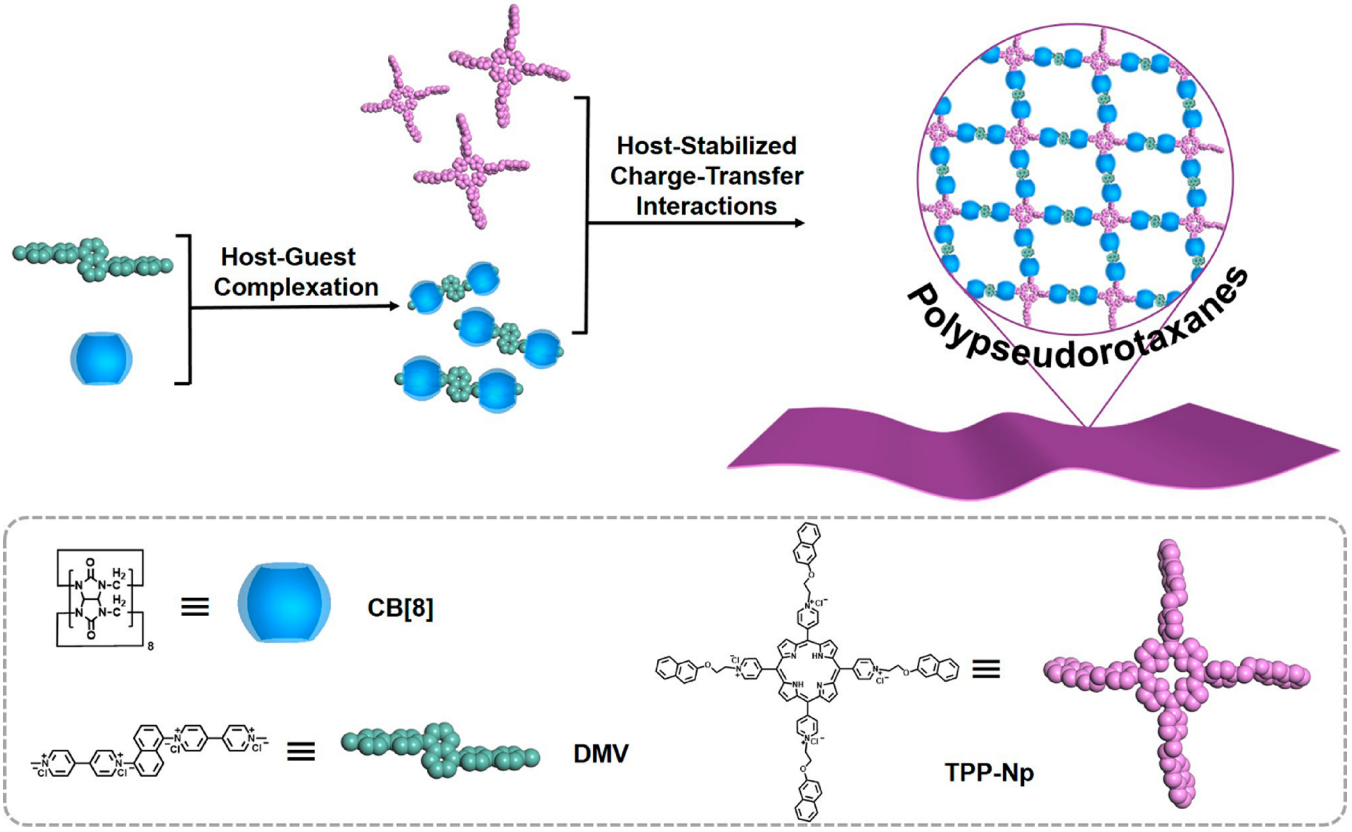

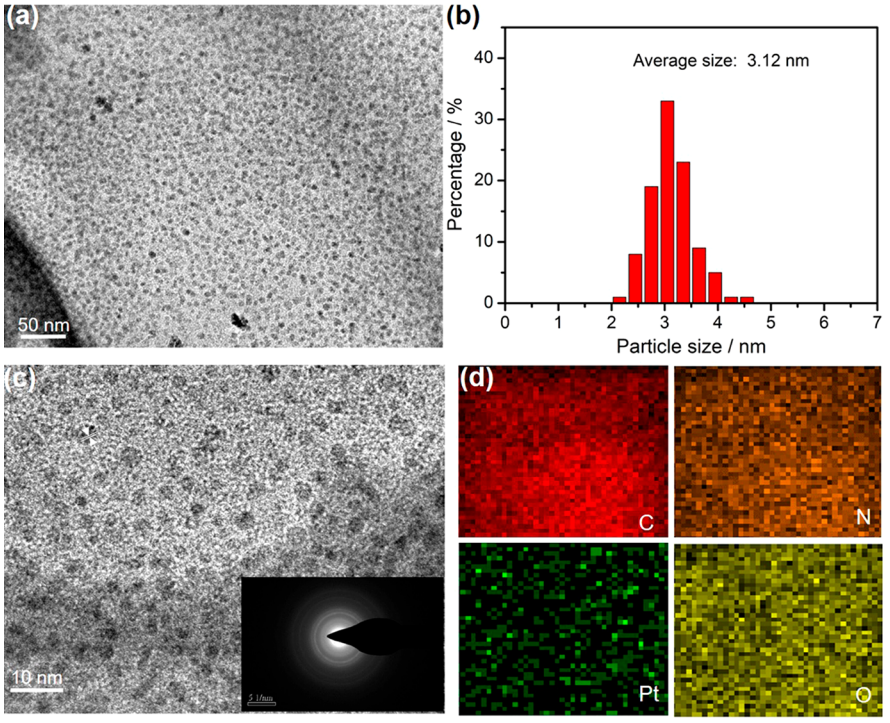

Figure 3. Characterization of 2D PtNPs@(CB[8]/DMV/TPP-Np). (a) Low-magnification TEM image of PtNPs@(CB[8]/DMV/TPP-Np). (b) Size distribution profile of Pt nanoparticles. (c) High-resolution TEM image of PtNPs@(CB[8]/DMV/TPP-Np). (d) TEM-EDS mapping of composition elements C, N, Pt, and O.

(NH_3) at atmospheric pressure and moderate temperature powered by renewable electricity has been an attractive subject of intense research.[32,33] Different from the current industrial Haber-Bosch process, which produces NH_3 from N_2 and H_2

https://dx.doi.org/10.1021/acs.chemmater.0c03425
Chem. Mater. 2020, 32, 8724−8732

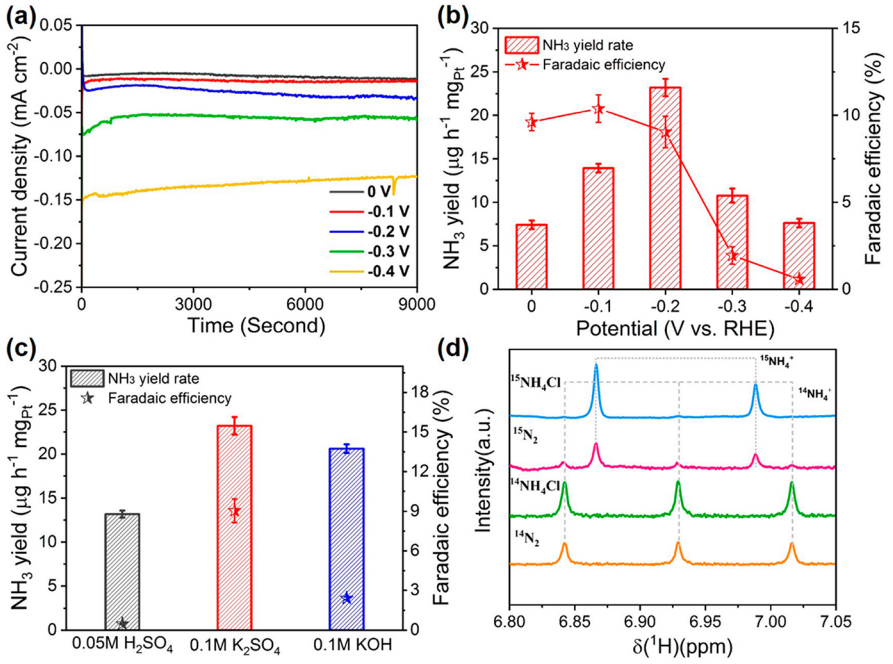

Figure 4. Electrocatalytic NRR activity of PtNPs@(CB[8]/DMV/TPP-Np). (a) Chronoamperometric curves at various potentials in N_2-saturated 0.1 M K_2SO_4. (b) NH_3 yields (left axis) and Faradaic efficiencies (FEs) (right axis) of PtNPs@(CB[8]/DMV/TPP-Np) at each given potential in 0.1 M K_2SO_4. The error bars correspond to the standard deviations of measurements over three separately prepared samples under the same conditions. (c) Corresponding NH_3 yield rates and Faradaic efficiencies in the three electrolytes at −0.2 V. (d) ^{15}N isotope labeling experiment. ^1H NMR spectra for the postelectrolysis 0.1 M K_2SO_4 electrolytes with $^{15}N_2$ and $^{14}N_2$ as the feeding gases. Also shown are the spectra for $^{15}NH^{4+}$ and $^{14}NH^{4+}$ standard samples.

catalyzed by iron-based catalysts under high temperature (350−550 °C) and high pressure (150−350 atm), the electrochemical NRR is considered a sustainable and promising approach for NH_3 production.[34,35] Recent reports illustrated that various materials including noble metals showed favorable activity for NH_3 production.[36,37] Significantly, we found that the Pt-based catalysts, which were thought to not be appropriate for NRR, could be efficient NRR catalysts.[38] Inspired by previous results and PtNPs@(CB[8]/DMV/TPP-Np) with high-density and finely dispersed Pt nanoparticles, extensive explorations and investigations toward the catalytic reactivity of hybrid materials for electrochemical NRR were conducted. To the best of our knowledge, there was no prior work based on supramolecular nanoarchitectures for nitrogen fixation, which is challenging but potentially valuable research.

The N_2 reduction activity of PtNPs@(CB[8]/DMV/TPP-Np) was carried out at room temperature and atmospheric pressure in an H-shaped electrochemical cell, which was separated by a Nafion membrane at room temperature and atmospheric pressure. The NRR activity of the electrode was evaluated using controlled potential electrolysis with N_2-saturated electrolytes. All potentials mentioned in this work were converted as the value versus RHE unless specified otherwise. The linear sweep voltammetry (LSV) curves of PtNPs@(CB[8]/DMV/TPP-Np) exhibited different current densities in the range from 0 to −0.70 V in 0.1 M K_2SO_4 solution with Ar-saturated and N_2-saturated electrolytes, respectively (Figure S24). The current density in N_2-saturated electrolyte is higher than that in Ar-saturated electrolyte, indicating that PtNPs@(CB[8]/DMV/TPP-Np) possesses catalytic activity toward N_2 electrochemical reduction.

The NH_3 yield rate was normalized on the basis of the weight of Pt loading. The produced NH_3 and N_2H_4 were measured according to the reported indophenol blue method and Watt and Chrisp method, respectively (the corresponding calibration curves are shown in Figures S25 and S26).[39,40] The production of hydrazine was below the detection limit, indicating high selectivity for NH_3 over PtNPs@(CB[8]/DMV/TPP-Np) (Figure S27). Time-dependent current density curves for 2.5 h from 0 to −0.4 V are presented in Figure 4a. The NH_3 yield and corresponding Faradaic efficiency revealed that the PtNPs@(CB[8]/DMV/TPP-Np) was an efficient catalyst for the fixation of inert N_2 molecules into valuable NH_3. As shown in Figure 4b, the NH_3 yield increased with more negative potential until −0.2 V, where the maximum value of the NH_3 yield was calculated as 23.2 $\mu g\ h^{-1}\ mg_{Pt}^{-1}$, and the Faradaic efficiency displayed the highest value of 10.39% at −0.1 V and then decreased gradually, which was ascribed to the competitive selectivity toward the hydrogen evolution reaction (HER).[41] For determination of the active sites of PtNPs@(CB[8]/DMV/TPP-Np) for electrocatalytic NRR, bare Pt nanoparticles and 2D polypseudorotaxanes as the controlled samples were also studied at the same catalytic potential (Figure S28). The results confirmed that the Pt nanoparticles with high density and fine dispersion in PtNPs@(CB[8]/DMV/TPP-Np) was the actual active sites for electroreduction of N_2 under ambient conditions. According to a previous report, Pt nanoparticles were stabilized by oxygen atoms at the edge of macrocycle structures of CB[8] and displayed positive charge, which can favorably chemisorb and activate the N_2.[38] In addition, macrocycle structures of CB[8] provided locally hydrophobic sites,[42] which is unfavorable to the HER process. As shown in Figure 4c, the findings of the electrocatalytic behaviors of PtNPs@(CB[8]/

https://dx.doi.org/10.1021/acs.chemmater.0c03425
Chem. Mater. 2020, 32, 8724−8732

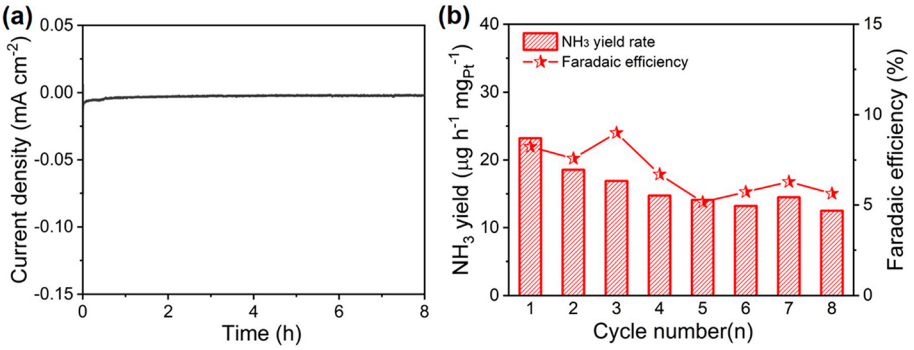

Figure 5. Stability tests. (a) Time-dependent current density curve. (b) Recycling test of PtNPs@(CB[8]/DMV/TPP-Np) at −0.2 V under ambient conditions.

DMV/TPP-Np) in different N_2-saturated electrolytes reveal that, compared with that in neutral electrolyte (0.1 M K_2SO_4, pH 7) at −0.2 V, the NH_3 yield and the Faradaic efficiency of PtNPs@(CB[8]/DMV/TPP-Np) were much lower than those in acid (0.05 M H_2SO_4, pH 1) and basic electrolytes (0.1 M KOH, pH 14), indicating that K_2SO_4 should be a promising electrolyte for electrochemical NRR because of its effective suppression of HER (Figure S29). Therefore, all of the following NRR experiments were conducted in 0.1 M K_2SO_4.

To confirm the origin of the produced NH_3, we carefully examined the nitrogen source through control experiments. First, the PtNPs@(CB[8]/DMV/TPP-Np) was immersed in a N_2-saturated electrolyte without applied potentials, and no NH_3 was detected using the indophenol blue method. Furthermore, the control experiments were carried out in Ar-saturated electrolyte at −0.2 V in 0.1 M K_2SO_4 solution, and only negligible NH_3 could be detected (Figure S30). And the pristine carbon paper was used as a working electrode in N_2-saturated electrolyte at −0.2 V in 0.1 M K_2SO_4 solution; no NH_3 was detected. The above experiment results suggest that the NH_3 was produced from electroreduction of N_2 by PtNPs@(CB[8]/DMV/TPP-Np). In addition, ^{15}N (99 atom % ^{15}N) isotopic labeling experiment was executed as an alternative method to verify the nitrogen source of the produced NH_3 generated in our experimental conditions.[36] As shown in Figure 4d, the standard samples illustrated a triplet coupling for $^{14}NH_4^+$ and a doublet coupling for $^{15}NH_4^+$ in ^1H NMR spectra. When $^{14}N_2$ or $^{15}N_2$ was supplied as the feeding gas, $^{14}NH_4^+$ or $^{15}NH_4^+$ could be detected, respectively, suggesting that the produced NH_3 originated from the electroreduction of N_2 instead of decomposition of catalysts or other contaminations.

The stability of the PtNPs@(CB[8]/DMV/TPP-Np) for electrochemical NRR was assessed by consecutive recycling electrolysis at −0.2 V. Under sustained N_2 gas flow, no obvious change in current density could be observed during electrolysis within 8 h. Furthermore, the catalytic activity displayed only a slight decrease in NH_3 yields and Faradaic efficiencies during eight consecutive cycles (Figure 5), suggesting that PtNPs@(CB[8]/DMV/TPP-Np) maintained satisfactory electrocatalytic activity. According to the high-resolution Pt XPS spectrum, the Pt chemical state of PtNPs@(CB[8]/DMV/TPP-Np) almost remained unchanged after electrocatalysis for NRR (Figure S31). The good stability of PtNPs@(CB[8]/DMV/TPP-Np) may be attributed to the strong host−guest interactions.

For investigation of the activation of N_2 on the surface of PtNPs@(CB[8]/DMV/TPP-Np) in our work, *in situ* time-resolved Fourier transform infrared (FTIR) spectroscopy was employed to demonstrate time-dependent changes of the N contained after injection of N_2. As shown in Figure 6a, the absorption band that can be assigned to $-N_2H_y$ intermediates gradually enhanced, exhibiting that N_2 can be efficiently adsorbed and activated on the surface of the PtNPs@(CB[8]/DMV/TPP-Np). More concretely, absorption bands appearing in the range from 1050 to 1500 cm^{-1} can be assigned to H−

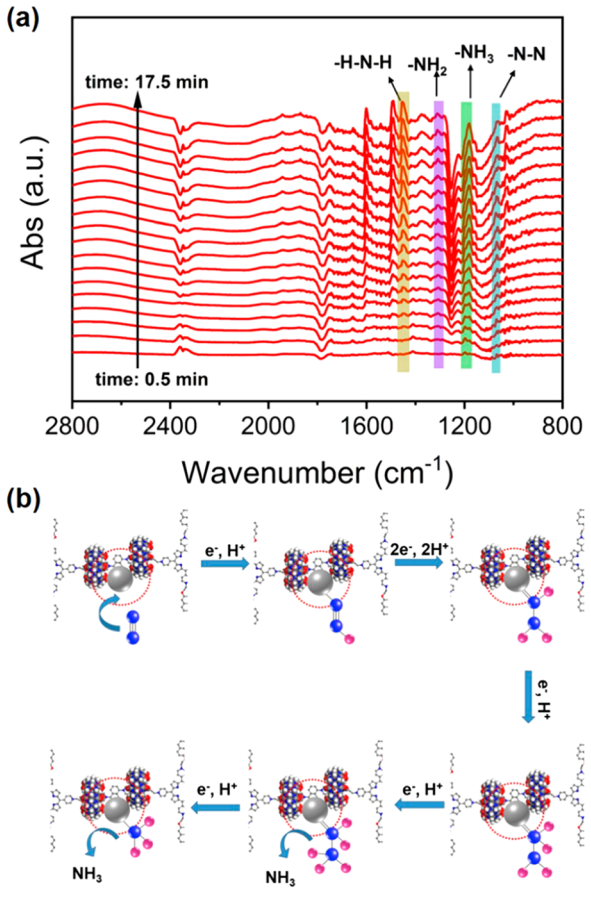

Figure 6. (a) Electrochemical in situ time-resolved Fourier transform infrared (FTIR) spectra for nitrogen reduction reaction (NRR) on the PtNPs@(CB[8]/DMV/TPP-Np) electrode. (b) Schematic illustration of the possible NRR process on the PtNPs@(CB[8]/DMV/TPP-Np) electrode.

https://dx.doi.org/10.1021/acs.chemmater.0c03425
Chem. Mater. 2020, 32, 8724−8732

N−H bending (1450 cm^{-1}), $-NH_2$ wagging (1301 cm^{-1}), adsorbed NH_3 (1200 cm^{-1}), and N−N stretching (1070 cm^{-1}) models of $-N_2H_y$ intermediates, respectively. The in situ time-resolved FTIR data provide strong evidence that the nitrogen reduction reaction on PtNPs@(CB[8]/DMV/TPP-Np) surfaces follows an associative mechanism.[43] Specifically, the possible NRR process over PtNPs@(CB[8]/DMV/TPP-Np) cathode can be reasonably deduced, as shown in Figure 6b. N_2 molecules were first adsorbed on the surface, and then the adsorbed N_2 reacted with the dissociated proton (H^+) from the electrolyte to form intermediates, resulting in the facilitation of dissociation of N≡N triple bonds.

CONCLUSIONS

In conclusion, novel 2D polypseudorotaxanes have been constructed by host-stabilized charge-transfer interactions by CB[8]. The functional and structural features allow the 2D supramolecular nanomaterial to be used as a platform for preparation of ultrafine Pt nanoparticles, which has been proven to pave a new way for electrochemical ammonia synthesis from nitrogen under ambient conditions with high yield and favorable stability. To the best of our knowledge, this is the first construction to realize artificial nitrogen fixation through supramolecular assembly strategy. As it is convenient, facile, and effective, the modular supramolecular assembly approach exhibits great potential for designing and constructing various functional 2D nanomaterials, which could give rise to new opportunities for electrochemical nitrogen reduction reaction and lead to various other applications.

EXPERIMENTAL SECTION

Preparation of PtNPs@CB[8]/DMV/TPP-Np. Platinum(II) solution was prepared by dissolving K_2PtCl_4 in water under ambient conditions and was aged 24 h before use; 125 μL of aqueous K_2PtCl_4 (20 mM), 10 mL solution of CB[8]/DMV/TPP-Np (0.05 mM of TPP-Np), and 125 μL of aqueous ascorbic acid (200 mM) were added into a glass vial together. The samples were irradiated by visible light through a 400 nm cutoff filter from a 300 W Xe lamp for 10 min.

Calculation of NH_3 Faradaic Efficiency (FE), NH_3 Yield Rate. The ammonia synthesis rate was calculated using the following equation:

$$\nu_{NH_3} = \frac{VC_{NH_3}}{m_{Pt}t}$$

FE was calculated according to the following equation:

$$FE = \frac{3Fn_{NH_3}}{Q}$$

where V is the volume of the electrolyte, C_{NH_3} is the NH_3 concentration, t is the reduction reaction time, A is the geometric area of the cathode, F is the Faraday constant, $m_{cat.}$ is the loading mass of the catalyst, and Q is the quantity of applied electricity.

Isotope-Labeled Experiments. The ^{14}N and ^{15}N isotopic labeling experiments were conducted using $^{14}N_2$ and $^{15}N_2$ as the feeding gases (99% enrichment of ^{15}N in $^{15}N_2$, supplied by Beijing Yinuokai Technology Co., Ltd.). Before the test was started, labeled $^{15}N_2$ gas was passed by alkaline solution (pH 14, KOH aqueous solution) and acid solution (pH 1, H_2SO_4 aqueous solution) to remove any N contamination before purging into the electrolyte solution. Because of the high price and small volume of $^{15}N_2$ gas bottles, we used a circulation setup in which $^{15}N_2$ gas was continuously cycled and resupplied to the electrode surface. Before flowing of $^{15}N_2$ gas, Ar gas was first flowed through the whole setup for 30 min to remove any $^{14}N_2$ gas that was present in the system, and then $^{15}N_2$ was flowed for 15 min. The NRR experiment was conducted at −0.2 V vs RHE for 6 h in 10 mL of 0.1 M K_2SO_4 aqueous solution in a circulation setup. Then 0.5 mL of the above solution mixed with 0.05 mL of d_6-DMSO was used for ^1H nuclear magnetic resonance (NMR) spectroscopy measurement (Bruker AVANCE III 600 MHz).

ASSOCIATED CONTENT

Supporting Information

The Supporting Information is available free of charge at https://pubs.acs.org/doi/10.1021/acs.chemmater.0c03425.

Characterizations of 2D polypseudorotaxanes and NRR catalytic performance of PtNPs@(CB[8]/DMV/TPP-Np), including NMR spectra, MS spectra, UV/vis spectra, and fluorescence spectra, SEM and AFM images, FT-IR and GI-SAXS patterns, LSV curves, and XPS spectra (PDF)

AUTHOR INFORMATION

Corresponding Authors

Yu Liu − *College of Chemistry, State Key Laboratory of Elemento-Organic Chemistry, Nankai University, Tianjin 300071, P.R. China;* orcid.org/0000-0001-8723-1896; Email: yuliu@nankai.edu.cn

Yu-Ping Liu − *College of Chemistry, Research Center for Analytical Sciences, Key Laboratory of Advanced Energy Materials Chemistry (Ministry of Education), Nankai University, Tianjin 300071, P.R. China*; Email: liuypnk@nankai.edu.cn

Authors

Cai-Cai Zhang − *College of Chemistry, State Key Laboratory of Elemento-Organic Chemistry, Nankai University, Tianjin 300071, P.R. China; College of Chemistry and Materials Science, Hebei Normal University, Shijiazhuang 050024, P.R. China.*

Xiaolu Liu − *College of Chemistry, Research Center for Analytical Sciences, Key Laboratory of Advanced Energy Materials Chemistry (Ministry of Education), Nankai University, Tianjin 300071, P.R. China*

Complete contact information is available at: https://pubs.acs.org/10.1021/acs.chemmater.0c03425

Author Contributions

#C.-C.Z. and X.L. contributed equally to this work.

Notes

The authors declare no competing financial interest.

ACKNOWLEDGMENTS

We thank the National Natural Science Foundation of China (Nos. 21432004, 21772099, and 21861132001) for financial support.

REFERENCES

(1) Liu, S.; Zhang, J.; Dong, R.; Gordiichuk, P.; Zhang, T.; Zhuang, X.; Mai, Y.; Liu, F.; Herrmann, A.; Feng, X. Two-Dimensional Mesoscale-Ordered Conducting Polymers. *Angew. Chem., Int. Ed.* **2016**, *55*, 12516−12521.

(2) Tan, C.; Cao, X.; Wu, X.-J.; He, Q.; Yang, J.; Zhang, X.; Chen, J.; Zhao, W.; Han, S.; Nam, G.-H.; Sindoro, M.; Zhang, H. Recent Advances in Ultrathin Two-Dimensional Nanomaterials. *Chem. Rev.* **2017**, *117*, 6225−6331.

(3) Wang, Y.; Li, Y.; Chen, Z. Planar Hypercoordinate Motifs in Two-Dimensional Materials. *Acc. Chem. Res.* **2020**, *53*, 887−895.

(4) Cai, S.-L.; Zhang, W.-G.; Zuckermann, R. N.; Li, Z.-T.; Zhao, X.; Liu, Y. The Organic Flatland—Recent Advances in Synthetic 2D Organic Layers. *Adv. Mater.* **2015**, *27*, 5762−5770.
(5) Muhabie, A. A.; Ho, C.-H.; Gebeyehu, B. T.; Huang, S.-Y.; Chiu, C.-W.; Lai, J.-Y.; Lee, D.-J.; Cheng, C.-C. Dynamic Tungsten Diselenide Nanomaterials: Supramolecular Assembly-Induced Structural Transition over Exfoliated Two-Dimensional Nanosheets. *Chem. Sci.* **2018**, *9*, 5452−5460.
(6) Cheng, Q.; Wu, H.; Zhang, H.; Yuan, S.; Hao, A.; Xing, P.; Zhao, Y. Ultrathin Supramolecular Architectures Self-Assembled from a C3-Symmetric Synthon for Selective Metal Binding. *ACS Appl. Mater. Interfaces* **2020**, *12*, 9673−9681.
(7) Zhang, Q.; Xing, R.-J.; Wang, W.-Z.; Deng, Y.-X.; Qu, D.-H.; Tian, H. Dynamic Adaptive Two-Dimensional Supramolecular Assemblies for On-Demand Filtration. *iScience* **2019**, *19*, 14−24.
(8) Zhang, K.-D.; Tian, J.; Hanifi, D.; Zhang, Y.; Sue, A. C.-H.; Zhou, T.-Y.; Zhang, L.; Zhao, X.; Liu, Y.; Li, Z.-T. Toward a Single-Layer Two-Dimensional Honeycomb Supramolecular Organic Framework in Water. *J. Am. Chem. Soc.* **2013**, *135*, 17913−17918.
(9) Pfeffermann, M.; Dong, R.; Graf, R.; Zajaczkowski, W.; Gorelik, T.; Pisula, W.; Narita, A.; Müllen, K.; Feng, X. Free-Standing Monolayer Two-Dimensional Supramolecular Organic Framework with Good Internal Order. *J. Am. Chem. Soc.* **2015**, *137*, 14525−14532.
(10) Sun, H.-L.; Chen, Y.; Han, X.; Liu, Y. Tunable Supramolecular Assembly and Photoswitchable Conversion of Cyclodextrin/Diphenylalanine-Based 1D and 2D Nanostructures. *Angew. Chem., Int. Ed.* **2017**, *56*, 7062−7065.
(11) Barrio, J. d.; Liu, J.; Brady, R. A.; Tan, C. S. Y.; Chiodini, S.; Ricci, M.; Fernandez-Leiro, R.; Tsai, C.-J.; Vasileiadi, P.; Di Michele, L.; Lairez, D.; Toprakcioglu, C.; Scherman, O. A. Emerging Two-Dimensional Crystallization of Cucurbit[8]uril Complexes: from Supramolecular Polymers to Nanofibers. *J. Am. Chem. Soc.* **2019**, *141*, 14021−14025.
(12) Dumele, O.; Chen, J.; Passarelli, J. V.; Stupp, S. I. Supramolecular Energy Materials. *Adv. Mater.* **2020**, *32*, 1907247.
(13) Liu, K.; Liu, Y.; Yao, Y.; Yuan, H.; Wang, S.; Wang, Z.; Zhang, X. Supramolecular Photosensitizers with Enhanced Antibacterial Efficiency. *Angew. Chem., Int. Ed.* **2013**, *52*, 8285−8289.
(14) Zhang, C.; Chen, P.; Dong, H.; Zhen, Y.; Liu, M.; Hu, W. Porphyrin Supramolecular 1D Structures via Surfactant-Assisted Self-Assembly. *Adv. Mater.* **2015**, *27*, 5379−5387.
(15) Geng, W.-C.; Zhang, D.; Gong, C.; Li, Z.; Barraza, K.; Beauchamp, J. L.; Guo, D.-S.; Zhang, X. Host-Guest Complexation of Amphiphilic Molecules at the Air-Water Interface Prevents Oxidation by Hydroxyl Radicals and Singlet Oxygen. *Angew. Chem., Int. Ed.* **2020**, *59*, 12684−12688.
(16) Fukui, T.; Kawai, S.; Fujinuma, S.; Matsushita, Y.; Yasuda, T.; Sakurai, T.; Seki, S.; Takeuchi, M.; Sugiyasu, K. Control over Differentiation of a Metastable Supramolecular Assembly in One and Two Dimensions. *Nat. Chem.* **2017**, *9*, 493−499.
(17) Jiang, H.; Zhang, L.; Chen, J.; Liu, M. Hierarchical Self-Assembly of a Porphyrin into Chiral Macroscopic Flowers with Superhydrophobic and Enantioselective Property. *ACS Nano* **2017**, *11*, 12453−12460.
(18) Sun, H.-L.; Chen, Y.; Zhao, J.; Liu, Y. Photocontrolled Reversible Conversion of Nanotube and Nanoparticle Mediated by β-Cyclodextrin Dimers. *Angew. Chem., Int. Ed.* **2015**, *54*, 9376−9380.
(19) Liu, G.; Zhang, Y.-M.; Xu, X.; Zhang, L.; Yu, Q.; Zhao, Q.; Zhao, C.; Liu, Y. Controllable Photoluminescence Behaviors of Amphiphilic Porphyrin Supramolecular Assembly Mediated by Cyclodextrins. *Adv. Opt. Mater.* **2017**, *5*, 1700770.
(20) Zhou, W.-L.; Zhao, X.; Chen, Y.; Liu, Y. Construction and Heterogeneous Photooxidization Reactivity of a Cyclodextrin/Porphyrin Polyrotaxane Network. *Org. Chem. Front.* **2019**, *6*, 10−14.
(21) Zhang, W.; Zhang, H.-Y.; Zhang, Y.-H.; Liu, Y. Fluorescent Supramolecular Polypseudorotaxane Architectures with Ru(ii)/Tri-(bipyridine) Centers as Multifunctional DNA Reagents. *Chem. Commun.* **2015**, *51*, 16127−16130.
(22) Kim, H.-J.; Heo, J.; Jeon, W. S.; Lee, E.; Kim, J.; Sakamoto, S.; Yamaguchi, K.; Kim, K. Selective Inclusion of a Hetero-Guest Pair in a Molecular Host: Formation of Stable Charge-Transfer Complexes in Cucurbit[8]uril. *Angew. Chem., Int. Ed.* **2001**, *40*, 1526−1529.
(23) Appel, E. A.; Biedermann, F.; Rauwald, U.; Jones, S. T.; Zayed, J. M.; Scherman, O. A. Supramolecular Cross-Linked Networks via Host-Guest Complexation with Cucurbit[8]uril. *J. Am. Chem. Soc.* **2010**, *132*, 14251−14260.
(24) Coulston, R. J.; Jones, S. T.; Lee, T.-C.; Appel, E. A.; Scherman, O. A. Supramolecular Gold Nanoparticle-Polymer Composites Formed in Water with Cucurbit[8]uril. *Chem. Commun.* **2011**, *47*, 164−166.
(25) Deng, W.; Onji, T.; Yamaguchi, H.; Ikeda, N.; Harada, A. Competitive Photoinduced Electron Transfer by the Complex Formation of Porphyrin with Cyclodextrin Bearing Viologen. *Chem. Commun.* **2006**, 4212−4214.
(26) Kim, J.; Jung, I.-S.; Kim, S.-Y.; Lee, E.; Kang, J.-K.; Sakamoto, S.; Yamaguchi, K.; Kim, K. New Cucurbituril Homologues: Syntheses, Isolation, Characterization, and X-ray Crystal Structures of Cucurbit-[n]uril (n = 5, 7, and 8). *J. Am. Chem. Soc.* **2000**, *122*, 540−541.
(27) Yin, H.; Tang, H.; Wang, D.; Gao, Y.; Tang, Z. Facile Synthesis of Surfactant-Free Au Cluster/Graphene Hybrids for High-Performance Oxygen Reduction Reaction. *ACS Nano* **2012**, *6*, 8288−8297.
(28) Wei, S.; Li, A.; Liu, J.-C.; Li, Z.; Chen, W.; Gong, Y.; Zhang, Q.; Cheong, W.-C.; Wang, Y.; Zheng, L.; Xiao, H.; Chen, C.; Wang, D.; Peng, Q.; Gu, L.; Han, X.; Li, J.; Li, Y. Direct Observation of Noble Metal Nanoparticles Transforming to Thermally Stable Single Atoms. *Nat. Nanotechnol.* **2018**, *13*, 856−861.
(29) Song, Y.; Yang, Y.; Medforth, C. J.; Pereira, E.; Singh, A. K.; Xu, H.; Jiang, Y.; Brinker, C. J.; van Swol, F.; Shelnutt, J. A. Controlled Synthesis of 2-D and 3-D Dendritic Platinum Nanostructures. *J. Am. Chem. Soc.* **2004**, *126*, 635−645.
(30) Liu, K.; Xing, R.; Chen, C.; Shen, G.; Yan, L.; Zou, Q.; Ma, G.; Möhwald, H.; Yan, X. Peptide-Induced Hierarchical Long-Range Order and Photocatalytic Activity of Porphyrin Assemblies. *Angew. Chem.* **2015**, *127*, 510−515.
(31) Lu, S.; Hu, Y.; Wan, S.; McCaffrey, R.; Jin, Y.; Gu, H.; Zhang, W. Synthesis of Ultrafine and Highly Dispersed Metal Nanoparticles Confined in a Thioether-Containing Covalent Organic Framework and Their Catalytic Applications. *J. Am. Chem. Soc.* **2017**, *139*, 17082−17088.
(32) van der Ham, C. J. M.; Koper, M. T. M.; Hetterscheid, D. G. H. Challenges in reduction of dinitrogen by proton and electron transfer. *Chem. Soc. Rev.* **2014**, *43*, 5183−5191.
(33) Chen, J. G.; Crooks, R. M.; Seefeldt, L. C.; Bren, K. L.; Bullock, R. M.; Darensbourg, M. Y.; Holland, P. L.; Hoffman, B.; Janik, M. J.; Jones, A. K.; Kanatzidis, M. G.; King, P.; Lancaster, K. M.; Lymar, S. V.; Pfromm, P.; Schneider, W. F.; Schrock, R. R. Beyond Fossil Fuel-Driven Nitrogen Transformations. *Science* **2018**, *360*, eaar6611.
(34) Ertl, G. Reactions at Surfaces: From Atoms to Complexity (Nobel Lecture). *Angew. Chem., Int. Ed.* **2008**, *47*, 3524−3535.
(35) Licht, S.; Cui, B.; Wang, B.; Li, F.-F.; Lau, J.; Liu, S. Ammonia Synthesis by N_2 and Steam Electrolysis in Molten Hydroxide Suspensions of Nanoscale Fe_2O_3. *Science* **2014**, *345*, 637−640.
(36) Wang, J.; Yu, L.; Hu, L.; Chen, G.; Xin, H.; Feng, X. Ambient Ammonia Synthesis via Palladium-Catalyzed Electrohydrogenation of Dinitrogen at Low Overpotential. *Nat. Commun.* **2018**, *9*, 1795.
(37) Tao, H.; Choi, C.; Ding, L.-X.; Jiang, Z.; Han, Z.; Jia, M.; Fan, Q.; Gao, Y.; Wang, H.; Robertson, A. W.; Hong, S.; Jung, Y.; Liu, S.; Sun, Z. Nitrogen Fixation by Ru Single-Atom Electrocatalytic Reduction. *Chem.* **2019**, *5*, 204−214.
(38) Hao, R.; Sun, W.; Liu, Q.; Liu, X.; Chen, J.; Lv, X.; Li, W.; Liu, Y.-P.; Shen, Z. Efficient Electrochemical Nitrogen Fixation over Isolated Pt Sites. *Small* **2020**, *16*, 2000015.
(39) Watt, G. W.; Chrisp, J. D. Sepectrophotometrc Method for Determination of Hydrzine. *Anal. Chem.* **1952**, *24*, 2006−2008.
(40) Zhu, D.; Zhang, L.; Ruther, R. E.; Hamers, R. J. Photo-Illuminated Diamond as a Solid-State Source of Solvated Electrons in Water for Nitrogen Reduction. *Nat. Mater.* **2013**, *12*, 836−841.

https://dx.doi.org/10.1021/acs.chemmater.0c03425
Chem. Mater. 2020, 32, 8724−8732

(41) Hao, Y.-C.; Guo, Y.; Chen, L.-W.; Shu, M.; Wang, X.-Y.; Bu, T.-A.; Gao, W.-Y.; Zhang, N.; Su, X.; Feng, X.; Zhou, J.-W.; Wang, B.; Hu, C.-W.; Yin, A.-X.; Si, R.; Zhang, Y.-W.; Yan, C.-H. Promoting Nitrogen Electroreduction to Ammonia with Bismuth Nanocrystals and Potassium Cations in Water. *Nat. Catal.* **2019**, *2*, 448−456.
(42) Biedermann, F.; Vendruscolo, M.; Scherman, O. A.; De Simone, A.; Nau, W. M. Cucurbit[8]uril and Blue-Box: High-Energy Water Release Overwhelms Electrostatic Interactions. *J. Am. Chem. Soc.* **2013**, *135*, 14879−14888.
(43) Song, P.; Wang, H.; Kang, L.; Ran, B.; Song, H.; Wang, R. Electrochemical Nitrogen Reduction to Ammonia at Ambient Conditions on Nitrogen and Phosphorus Co-doped Porous Carbon. *Chem. Commun.* **2019**, *55*, 687−690.

https://dx.doi.org/10.1021/acs.chemmater.0c03425
Chem. Mater. 2020, 32, 8724−8732